

Model-Free Analysis of Protein Backbone Motion from Residual Dipolar Couplings

Wolfgang Peti,^{†,§} Jens Meiler,^{†,⊥} Rafael Brüschweiler,[‡] and Christian Griesinger^{*,†}

Contribution from the Max-Planck Institute for Biophysical Chemistry, Am Fassberg 11, D-37077 Göttingen, Germany, and Gustaf H. Carlson School of Chemistry and Biochemistry, Clark University, 950 Main Street, Worcester, Massachusetts 01610-1477

Received August 3, 2001. Revised Manuscript Received November 14, 2001

Abstract: On the basis of the measurement of NH residual dipolar couplings (RDCs) in 11 different alignment media, an RDC-based order parameter is derived for each residue in the protein ubiquitin. Dipolar couplings are motionally averaged in the picosecond to millisecond time range and, therefore, reflect motion slower than the inverse overall tumbling correlation time of the protein. It is found that there is considerable motion that is slower than the correlation time and could not be detected with previous NMR methodology. Amplitudes and anisotropies of the motion can be derived from the model-free analysis. The method can be applied provided that at least five sufficiently different alignment media can be found for the biomolecule under investigation.

Introduction

Over the past few years, residual dipolar couplings (RDCs)^{1,2} have emerged as highly useful NMR parameters for the elucidation and refinement of biomolecular structures in solution. RDCs complement the traditional NMR parameters such as NOE and scalar couplings, as well as other new types of constraints such as cross-correlated relaxation parameters³ and trans-hydrogen bond *J* couplings,⁴ since they provide long-range structural restraints.

One of the most important applications of RDCs aims at the reduction of the number of required NOEs for determining the 3D structure of a protein.^{5–9} In another use of RDCs, the PDB database is searched for protein structures that are consistent with a given set of RDCs.^{10–13} Using another approach, structures of protein fragments are identified from the database, and the 3D backbone structure of the protein is then reconstructed by properly assembling these fragments.¹⁴ Taking it a step further, it was demonstrated that the backbone structure of ubiquitin can be determined by aligning sequential peptide planes solely on the basis of RDCs, that is, without using database information.¹⁵

It was recognized early on that dipolar couplings not only reflect the average structure but also structural fluctuations

allowing the characterization of conformational flexibility in proteins.¹⁶ For cyanometmyoglobin, which contains eight helices, Tolman et al.^{17,18} presented two dynamical models to reproduce the experimental dipolar couplings.^{1,18,19} The dynamical models were based on structures obtained by X-ray,²⁰ neutron diffraction,²¹ and NMR.²² The first model describes motions of the helices as a cooperative wobbling in a cone with symmetry axis along the helix axes. In the second model, the helix was treated as a rigid unit that undergoes rotations about an axis perpendicular to the helix axis. In both models, scaling

* To whom correspondence should be addressed. E-mail: cigr@nmr.mpibpc.mpg.de.

[†] Max-Planck Institute for Biophysical Chemistry.

[‡] Clark University.

[§] Current address: The Scripps Research Institute, Department of Molecular Biology, and The Skaggs Institute of Biological Chemistry, 10550 North Torrey Pines Road, La Jolla, CA 92037.

[⊥] Current address: University of Washington, Department of Biochemistry, Box 357350, Seattle, WA 98195.

(1) Tolman, J. R.; Flanagan, J. M.; Kennedy, M. A.; Prestegard, J. H. *Proc. Natl. Acad. Sci. U.S.A.* **1995**, *92*, 9279–9283.

(2) Tjandra, N.; Bax, A. *Science* **1997**, *278*, 1111–1114.

(3) Reif, B.; Hennig, M.; Griesinger, C. *Science* **1997**, *276*, 1230–1233.

(4) Dingley, A. J.; Grzesiek, S. *J. Am. Chem. Soc.* **1998**, *120*, 8293–8297.

(5) Drohat, A. C.; Tjandra, N.; Baldisseri, D. M.; Weber, D. *J. Protein Sci.* **1999**, *8*, 800–809.

(6) Bewley, C. A.; Gustafson, K. R.; Boyd, M. R.; Covell, D. G.; Bax, A.; Clore, G. M.; Gronenborn, A. M. *Nat. Struct. Biol.* **1998**, *5*, 571–578.

(7) Cai, M.; Huang, Y.; Zheng, R.; Wei, S.-Q.; Ghirlando, R.; Lee, M. S.; Craigie, R.; Gronenborn, A. M.; Clore, G. M. *Nat. Struct. Biol.* **1998**, *5*, 903–909.

(8) Clore, G. M.; Straich, M. R.; Bewley, C. A.; Cai, M.; Kuszewski, J. *J. Am. Chem. Soc.* **1999**, *121*, 6513–6514.

(9) Meiler, J.; Blomberg, N.; Nilges, M.; Griesinger, C. *J. Biomol. NMR* **2000**, *16*, 245–252.

(10) Aitio, H.; Annala, A.; Heikkinen, S.; Thulin, E.; Drakenberg, T.; Kilpeläinen, I. *Protein Sci.* **1999**, *8*, 2580–2588.

(11) Andrec, M.; Du, P.; Levy, R. M. *J. Am. Chem. Soc.* **2001**, *123*, 1222–1229.

(12) Annala, A.; Aitio, H.; Thulin, E.; Drakenberg, T. *J. Biomol. NMR* **1999**, *14*, 223–230.

(13) Meiler, J.; Peti, W.; Griesinger, C. *J. Biomol. NMR* **2000**, *17*, 283–294.

(14) Delaglio, F.; Kontaxis, G.; Bax, A. *J. Am. Chem. Soc.* **2000**, *122*, 2142–2143.

(15) Hus, J.-C.; Marion, D.; Blackledge, M. *J. Am. Chem. Soc.* **2001**, *123*, 1541–1542.

(16) Tolman, J. R.; Flanagan, J. M.; Kennedy, M. A.; Prestegard, J. H. *Nat. Struct. Biol.* **1997**, *4*, 292–297.

(17) Prestegard, J. H.; Tolman, J. R.; Al-Hashimi, H. M.; Andrec, M. *Protein Structure and Dynamic from Field-Induced Residual Dipolar Couplings*; Kluwer Academic/Plenum Press: New York, 1999; Vol. 17.

(18) Tolman, J. R.; Prestegard, J. H. *J. Magn. Reson., Ser. B* **1996**, *112*, 245–252.

(19) Tolman, J. R.; Prestegard, J. H. *J. Magn. Reson., Ser. B* **1996**, *112*, 269–274.

(20) Kuriyan, J.; Wilz, S.; Karplus, M.; Petsko, G. A. *J. Mol. Biol.* **1986**, *192*, 133–154.

(21) Cheng, X.; Schoenborn, B. P. *J. Mol. Biol.* **1991**, *220*, 381–399.

(22) Osapay, K.; Theriault, Y.; Wright, P. E.; Case, D. A. *J. Mol. Biol.* **1994**, *244*, 183–197.

Table 1. Comparison of the Singular Values and the Condition Numbers for the 5–11 Best Alignment Media^a

number of used alignment conditions	5	6	7	8	9	10	11
DMPC/DHPC	0	1	1	1	1	1	1
DMPC/DHPC/SDS	0	0	0	0	0	0	1
purple membrane fragments	1	1	1	1	1	1	1
CHAPSO/DLPC/SDS	0	1	1	1	1	1	1
CHAPSO/DLPC	1	0	0	0	1	1	1
CHAPSO/DPLC/CTAB 4%	0	0	1	1	1	1	1
CHAPSO/DPLC/CTAB 5%	0	0	0	0	0	1	1
polyacrylamide gel	0	0	0	1	1	1	1
Helfrich phase	1	1	1	1	1	1	1
Pf-1 phages	1	1	1	1	1	1	1
<i>n</i> -dodecyl-penta(ethylene glycol)/ <i>n</i> -hexanol	1	1	1	1	1	1	1
condition number	6.362	6.184	6.548	7.039	7.367	7.817	8.267
singular value 1	3.045	3.373	3.759	4.094	4.333	4.617	4.909
singular value 2	1.804	1.898	2.013	2.071	2.203	2.220	2.260
singular value 3	0.618	0.723	0.725	0.775	0.796	0.833	0.844
singular value 4	0.532	0.600	0.600	0.646	0.646	0.675	0.675
singular value 5	0.479	0.546	0.574	0.582	0.588	0.591	0.594

^a In all cases with less than 11 alignments, the combination of the alignment media is given that provides the largest fifth singular value. The smallest singular value of the \bar{F} matrix is most significant for the propagation of errors into the model-free analysis. Thus, six experimental alignment tensors are almost as good as 11 for the purposes of this paper.

factors S for the dipolar couplings were introduced that decreased dipolar couplings predicted from a static structure. The extracted scaling factors varied between 0.45 and 0.7 for individual helices, corresponding to sizable cone opening angles (e.g., $\alpha = 42^\circ$ for $S = 0.65$) if axially symmetric motions are assumed.

More recently, Tolman et al. presented an approach to extract dynamics from a set of RDCs measured along the backbone of ubiquitin.²³ They used a single alignment medium and measured seven different heteronuclear dipolar couplings, including the spin pairs N–HN, C^i –HN^(*i*+1), C^i –N^(*i*+1), $C\alpha$ –C', C'–H α , $C\alpha$ –H α , and $C\alpha$ –C β within the backbone of each amino acid. Assuming a fixed geometry of these vectors for each amino acid moiety in the protein, they derived a general degree of order value ϑ (GDO) that reflects the motional scaling of the dipolar couplings for each peptide moiety. The success of the approach, however, critically depends on the accurate knowledge of the local bonding geometry of all atoms involved (bond lengths and bond angles) and on the φ torsion angle.

Recently, we introduced a “model-free” approach to the dynamic interpretation of RDCs of a single dipolar vector measured in multiple alignments.²⁴ The approach used a 10 ns molecular dynamics (MD) simulation of ubiquitin from which averaged RDCs were computed for backbone NH dipolar vectors using nine different alignments. A mathematical framework was developed that describes the extraction of averages of spherical harmonics of rank 2, $\langle Y_{2M}(\theta, \phi) \rangle$, and of effective vector orientations ($\theta_{\text{eff}}, \phi_{\text{eff}}$) that correspond in good approximation to the average orientations ($\theta_{\text{av}}, \phi_{\text{av}}$) as extracted from the trajectory. The $\langle Y_{2M}(\theta, \phi) \rangle$ quantities reflect motional averaging without necessitating a concrete motional model, in analogy to the model-free approach of Lipari and Szabo^{25,26} used for the interpretation of NMR spin relaxation data. The $\langle Y_{2M}(\theta, \phi) \rangle$ can be used to calculate an S_{rdc}^2 order parameter that is similar to the Lipari and Szabo S_{LS}^2 order parameter with the important difference that S_{rdc}^2 reflects motions on a time-scale range

between femtoseconds and milliseconds, while S_{LS}^2 reflects motions on (sub-) nanosecond time scales.

In the past, motions on time scales of microseconds to milliseconds were primarily accessed using $T_{1\rho}$ measurements. Off-resonance $T_{1\rho}$ experiments further extend the accessible time-scale range.^{27,28} The translation of $T_{1\rho}$ data into dynamic models is hampered by the fact that the chemical shift information of the different conformers does not allow the derivation of structural models of the interconverting conformers. Therefore, additional dynamic information is highly desirable to characterize structural processes on these slow time scales. In addition, scalar J couplings also provide detailed information on slow time-scale motion.²⁹

Here we apply the theoretical approach of Meiler et al.²⁴ to experimental NH dipolar couplings of ubiquitin. Ubiquitin is perhaps the protein that is best studied by NMR. Numerous ¹⁵N backbone relaxation studies have been reported.^{30–33} Using different approaches, it is well established that in ubiquitin only the residues I23 and N25 exhibit conformational exchange.^{31,34,35} H–D exchange data are also available for ubiquitin.^{36,37} Residual dipolar coupling data were published for bicelle media.^{23,38,39} In this work RDCs of ubiquitin are measured for 11 different alignment media used to probe intramolecular motions in a model-free way (see Table 1). The data are interpreted using

- (23) Tolman, J. R.; Al-Hashimi, H. M.; Kay, L. E.; Prestegard, J. H. *J. Am. Chem. Soc.* **2001**, *123*, 1416–1424.
 (24) Meiler, J.; Prompers, J. J.; Peti, W.; Griesinger, C.; Brüschweiler, R. *J. Am. Chem. Soc.* **2001**, *123*, 6098–6107.
 (25) Lipari, G.; Szabo, A. *J. Am. Chem. Soc.* **1982**, *104*, 4546–4559.
 (26) Lipari, G.; Szabo, A. *J. Am. Chem. Soc.* **1982**, *104*, 4559–4570.

- (27) Akke, M.; Liu, J.; Cavanagh, J.; Erickson, H. P.; Palmer, A. G. *Nat. Struct. Biol.* **1998**, *5*, 55–59.
 (28) Zinn-Justin, S.; Berhault, P.; Guenneugues, M.; Desvaux, H. *J. Biomol. NMR* **1997**, *10*, 363–372.
 (29) Case, D. A.; Scheurer, C.; Brüschweiler, R. *J. Am. Chem. Soc.* **2000**, *122*, 10390–10397.
 (30) Schneider, D. M.; Dellwo, M. J.; Wand, A. J. *Biochemistry* **1992**, *31*, 3645–3652.
 (31) Tjandra, N.; Feller, S. E.; Pastor, R. W.; Bax, A. *J. Am. Chem. Soc.* **1995**, *117*, 12562–12566.
 (32) Lienin, S. F.; Bremi, T.; Brutscher, B.; Brüschweiler, R.; Ernst, R. R. *J. Am. Chem. Soc.* **1998**, *120*, 9870–9879.
 (33) Carlomagno, T.; Maurer, M.; Hennig, M.; Griesinger, C. *J. Am. Chem. Soc.* **2000**, *122*, 5105–5113.
 (34) Tjandra, N.; Szabo, A.; Bax, A. *J. Am. Chem. Soc.* **1996**, *118*, 6986–6991.
 (35) de Alba, E.; Baber, J. L.; Tjandra, N. *J. Am. Chem. Soc.* **1999**, *121*, 4282–4283.
 (36) Johnson, E. C.; Lazar, G. A.; Desjarlais, J. R.; Handel, T. M. *Structure* **1999**, *7*, 967–976.
 (37) Sivaraman, T.; Arrington, C. B.; Robertson, A. D. *Nat. Struct. Biol.* **2001**, *8*, 331–333.
 (38) Cornilescu, G.; Marquardt, J. L.; Ottiger, M.; Bax, A. *J. Am. Chem. Soc.* **1999**, *121*, 6836–6837.
 (39) Ottiger, M.; Bax, A. *J. Am. Chem. Soc.* **1998**, *120*, 12334–12341.

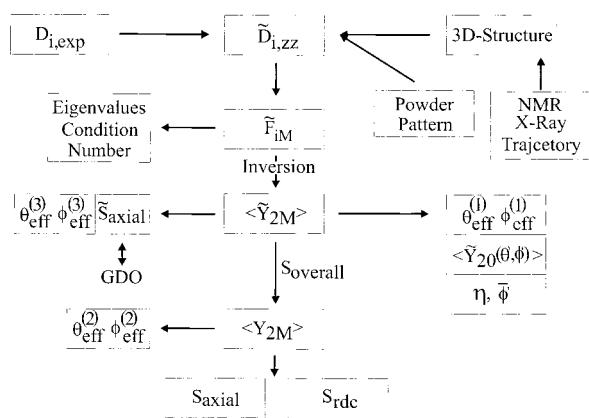


Figure 1. Overview of the most important steps to extract structural and model-free dynamical information from dipolar couplings. D_i^{exp} is the experimental dipolar couplings measured in i different alignment media; $\tilde{D}_{i,zz}$ is the largest principal component of the alignment tensor extracted from the experimental data using a rigid model (NMR, X-ray, or trajectory); $F_{i,M}$ are elements of \hat{F} matrix including all the alignment tensor information and the Wigner rotation elements for the translation from the individual alignment frames to the molecular frame; $\langle \tilde{Y}_{2M} \rangle$ are the spherical harmonic functions derived from the experimental dipolar couplings; $\theta_{\text{eff}}^{(1,2,3)}$, $\phi_{\text{eff}}^{(1,2,3)}$ are the effective orientations of the NH vectors derived using three different approaches. The first approach is used for the model-free analysis. $\langle Y_{20}(\theta', \phi') \rangle$ is the isotropic part of the motion; η and $\bar{\phi}'$ are the amplitude and the orientation of the anisotropic motion, respectively. S_{overall} is the overall scaling factor that reflects the overall scaling of the back calculated alignment tensors due to motion; S_{axial} is the residue specific order parameter describing the axially symmetric motion; S_{rdc} is the dipolar order parameter. Details can additionally be found in the text of the manuscript.

the framework described in the theory paper²⁴ yielding effective NH vector orientations, fluctuation amplitudes expressed in terms of the RDC-derived order parameter S_{rdc}^2 , and information about the asymmetry of intramolecular motions. Adaptations of the introduced mathematical analysis that proved to be useful in the context of experimental data are summarized in the following section and in the flowchart given in Figure 1.

Theoretical Results. The dipolar couplings observed in a certain anisotropic medium (denoted by index i) are given by

$$D_i^{\text{exp}} = D_{i,zz} \left\{ 3 \cos^2 \theta_i^{\text{at}} - 1 \right\} + \frac{3}{2} R_i \left\{ \sin^2 \theta_i^{\text{at}} \cos 2\phi_i^{\text{at}} \right\} \quad (1)$$

The angular brackets denote conformational averaging. $D_{i,zz}$ is the main component, and R_i is the rhombicity of the alignment tensor. θ^{at} and ϕ^{at} are the orientations of the vectors in the frame of the alignment tensor (at). To analyze dipolar couplings in the context of dynamics it is useful to express eq 1 using normalized second-order spherical harmonic functions as given in eq 2 (a more detailed description is given in the Appendix):

$$\frac{D_i^{\text{exp}}}{D_{i,zz}} = \sum_{M=-2}^2 F_{i,M} \langle Y_{2,M}(\theta^{\text{mol}}, \phi^{\text{mol}}) \rangle \quad (2)$$

where $\langle Y_{2M}(\theta, \phi) \rangle$ are the averaged spherical harmonics for a given NH vector. The superscript mol in eq 2 describes the change of the coordinate system from the alignment tensor frame into the molecular frame. The $F_{i,M}$ are functions of the three Euler angles, α_i , β_i , and γ_i , that relate the molecular frame to the dipolar frame (see Appendix). In the following, we will use θ and ϕ where we refer to the molecular frame of the protein.

We have shown in the theory paper in scenario II that fitting the dipolar couplings to NH vectors contained in secondary structure elements of one rigid NMR structure⁴⁰ will yield a motion averaged alignment tensor characterized by $\tilde{D}_{i,zz}$ and \tilde{R}_i as well as the angles $\tilde{\alpha}_i$, $\tilde{\beta}_i$, and $\tilde{\gamma}_i$. The orientation $(\tilde{\alpha}_i, \tilde{\beta}_i, \tilde{\gamma}_i)$ and the rhombicity (\tilde{R}_i) of the scaled tensor are virtually indistinguishable from those of the true tensor, and the motion is reflected only in a scaling of the principal value according to $\tilde{D}_{i,zz} = S_{\text{overall}} \cdot D_{i,zz}$ ($S_{\text{overall}} = \lambda_{\text{overall}}$ in scenario II in the theory paper). The rhombicity and the orientation of the scaled versus the true tensor were independent of the exact value of the overall scaling, as well as the structure used for fitting the tensor, provided that the column vectors \tilde{F}_i derived from the \hat{F} matrix are sufficiently linearly independent from each other. We can thus rewrite eq 2 on the basis of the experimentally scaled alignment tensor using scaled spherical harmonics $\langle \tilde{Y}_{2M}(\theta, \phi) \rangle$:

$$\frac{D_i^{\text{exp}}}{\tilde{D}_{i,zz}} = \sum_{M=-2}^2 F_{i,M} \langle \tilde{Y}_{2,M}(\theta^{\text{mol}}, \phi^{\text{mol}}) \rangle = \sum_{M=-2}^2 F_{i,M} \langle \langle Y_{2,M}(\theta^{\text{mol}}, \phi^{\text{mol}}) \rangle / S_{\text{overall}} \rangle \quad (3)$$

Model-Free Approach. The inversion of the \hat{F} matrix in eq 3 yields the averages of the spherical harmonics. Because we enforce $\langle Y_{22}(\theta, \varphi) \rangle^* \stackrel{!}{=} \langle Y_{2-2}(\theta, \varphi) \rangle$ and $\langle Y_{21}(\theta, \varphi) \rangle^* \stackrel{!}{=} -\langle Y_{2-1}(\theta, \varphi) \rangle$ in eq 3, five independent variables remain for the calculation. Therefore, we need at least five alignments that must be realized experimentally to calculate the $\langle Y_{2M}(\theta, \phi) \rangle$ values. However, from eq 3 we only obtain $\langle Y_{2M}(\theta, \phi) \rangle / S_{\text{overall}} = \langle \tilde{Y}_{2M}(\theta, \phi) \rangle$ and not the desired $\langle Y_{2M}(\theta, \phi) \rangle$ values. We therefore need to determine S_{overall} as will be described in the course of the paper. The $\langle Y_{2M}(\theta, \phi) \rangle$ values yield a model-free analysis of the motion and make a detailed picture of the motion available than is provided by S_{LS}^2 , the Lipari–Szabo order parameter.

To achieve this more detailed picture we rotate each individual NH vector into a frame with primed axes x', y', z' such that $\langle \tilde{Y}_{20}(\theta', \phi') \rangle$ is maximized:

$$\max \stackrel{!}{=} \langle \tilde{Y}_{20}(\theta', \phi') \rangle = \sum_{M=-2}^2 D_{M,0}(\phi_{\text{eff}}^{(1)}, \theta_{\text{eff}}^{(1)}) \langle \tilde{Y}_{2M}(\theta, \phi) \rangle = \sqrt{\frac{4\pi}{5}} \sum_{M=-2}^2 Y_{2,-M}(\theta_{\text{eff}}^{(1)}, \phi_{\text{eff}}^{(1)}) \langle \tilde{Y}_{2M}(\theta, \phi) \rangle \quad (4)$$

Maximizing $\langle \tilde{Y}_{20}(\theta', \phi') \rangle$ puts the new z' axis into the center of the distribution for the given NH vector and thus defines $\theta_{\text{eff}}^{(1)}$ and $\phi_{\text{eff}}^{(1)}$. As shown in the Appendix, the $\langle \tilde{Y}_{21}(\theta', \phi') \rangle$ and $\langle \tilde{Y}_{2-1}(\theta', \phi') \rangle$ values vanish. The $\langle \tilde{Y}_{22}(\theta', \phi') \rangle$ and $\langle \tilde{Y}_{2-2}(\theta', \phi') \rangle$ averages then reflect the asymmetry of the motion. To derive parameters that are easier to grasp, we define a relative amplitude η of anisotropy of the motion defined in eq 5 that is equivalent to the definition of η in the theoretical paper (eq 11). This η parameter is independent of the overall scaling S_{overall} :

(40) Cornilescu, G.; Marquardt, J. L.; Ottiger, M.; Bax, A. *PDB Database*, 1999, 1D3Z.

$$\eta = \frac{\sqrt{\sum_{M=-2,2} \langle \tilde{Y}_{2M}(\theta', \phi') \rangle \langle \tilde{Y}_{2-M}(\theta', \phi') \rangle}}{\sqrt{\sum_{M=-2}^2 \langle \tilde{Y}_{2M}(\theta', \phi') \rangle \langle \tilde{Y}_{2-M}(\theta', \phi') \rangle}} \quad (5)$$

The ratio of the imaginary and the real part of $\langle \tilde{Y}_{22}(\theta', \phi') \rangle$ and $\langle \tilde{Y}_{2-2}(\theta', \phi') \rangle$ defines the orientation of the anisotropic motion.

$$\bar{\phi}' = \frac{1}{2} \arctan \frac{\langle \tilde{Y}_{22}(\theta', \phi') \rangle - \langle \tilde{Y}_{2-2}(\theta', \phi') \rangle}{i(\langle \tilde{Y}_{22}(\theta', \phi') \rangle + \langle \tilde{Y}_{2-2}(\theta', \phi') \rangle)} \quad (6)$$

It should be noted that due to the ϕ dependence of the $Y_{22}(\theta, \phi)$ and $Y_{2-2}(\theta, \phi)$ functions, the $\bar{\phi}'$ angle has a π periodicity. It is obvious from the definition of $\bar{\phi}'$ that it is different from the average ϕ' of a distribution of vector orientations $\langle \phi' \rangle$. The translation of the five averaged spherical harmonics into the primed coordinate system amounts to the definition of five new parameters: $\langle \tilde{Y}_{20}(\theta', \phi') \rangle$ which reflects the axial order, $\theta_{\text{eff}}^{(1)}$ and $\phi_{\text{eff}}^{(1)}$ which reflect the average orientation of the vector, and η and $\bar{\phi}'$ which reflect the amount of anisotropic disorder and the direction of this anisotropic motion in the x', y' plane.

In addition to dissecting the orientational disorder into its axially symmetric and asymmetric distribution, we can also calculate a traditional order parameter S_{rdc}^2 that is based exclusively on dipolar couplings and formulated in analogy to the well-known Lipari–Szabo order parameter:²⁵

$$S_{\text{rdc}}^2 = \frac{4\pi}{5} \sum_{M=-2}^2 \langle Y_{2M}(\theta, \phi) \rangle \langle Y_{2M}^*(\theta, \phi) \rangle \quad (7)$$

In contrast to S_{LS}^2 , S_{rdc}^2 covers motion up to the NMR time scale that is defined by the inverse of the differences of chemical shifts or dipolar couplings of exchanging conformations. It should be noted that the S_{rdc}^2 values form a distribution with an average of S_{overall}^2 and that they are always smaller than 1. Consequently, the \tilde{S}_{rdc}^2 values derived from the $\langle \tilde{Y}_{2M}(\theta, \phi) \rangle$ form a distribution with an average of 1, and therefore certain \tilde{S}_{rdc}^2 will exceed 1 for some of the NH vectors.

Derivation of Average Orientations. In the theoretical paper we were interested in the calculation of the averaged orientations of the vectors $(\theta_{\text{av}}, \phi_{\text{av}})$ defined as the polar angles of an averaged NH vector over the trajectory. We found that these can be obtained very accurately from the averages of the spherical harmonics $\langle Y_{2M}(\theta, \phi) \rangle$ and even better from the experimentally directly accessible $\langle Y_{2M}(\theta, \phi) \rangle / S_{\text{overall}} = \langle \tilde{Y}_{2M}(\theta, \phi) \rangle$. There are several options to derive these effective angles θ_{eff} and ϕ_{eff} which we call effective instead of average since they are not identical with the averages.

The first approach for the optimization of $\theta_{\text{eff}}, \phi_{\text{eff}}$ uses the average spherical harmonics $\langle \tilde{Y}_{2M}(\theta, \phi) \rangle$ obtained by eq 3 and rotates them into a primed reference frame in which the new average $\langle \tilde{Y}_{20}(\theta', \phi') \rangle$ is maximized according to eq 4. This approach was already explained in the previous paragraph. The superscript 1 on $\theta_{\text{eff}}, \phi_{\text{eff}}$ in eq 4 indicates that this is just the first way to derive the information about the effective $\theta_{\text{eff}}, \phi_{\text{eff}}$. It is obvious that $\langle \tilde{Y}_{20}(\theta, \phi) \rangle$ is at a maximum when the average vector is parallel to the z -axis. This approach is used to derive the motional models from the averaged spherical harmonics (eqs 5 and 6).

The second approach is to find two angles θ_{eff} and ϕ_{eff} that minimize the following expression:

$$\sum_{M=-2}^2 (\langle Y_{2M}(\theta, \phi) \rangle - Y_{2M}(\theta_{\text{eff}}^{(2)}, \phi_{\text{eff}}^{(2)}))^2 \quad (8)$$

It has the drawback that individual order parameters for each NH vector are not taken into account.

Therefore, a third approach is used, in which the directly accessible $\langle \tilde{Y}_{2M}(\theta, \phi) \rangle$ values are scaled assuming axially symmetric motion. The scaling factor $\tilde{S}_{\text{axial}} = S_{\text{axial}}/S_{\text{overall}}$ is individually optimized for each NH vector but uniform for all alignment media. The subscript “axial” is used for this parameter since the value enforces a uniform scaling of all spherical harmonic $\langle \tilde{Y}_{2M}(\theta, \phi) \rangle$ values and therefore a uniform scaling of all experimental dipolar couplings. This is true for axially symmetric motion as discussed in the theory paper.

$$\sum_{M=-2}^2 (\langle \tilde{Y}_{2M}(\theta, \phi) \rangle / \tilde{S}_{\text{axial}} - Y_{2M}(\theta_{\text{eff}}^{(3)}, \phi_{\text{eff}}^{(3)}))^2 \quad (9)$$

Comparison with GDO Approach. The scaling by S_{axial} is very similar to the internal generalized degree of order (GDO) analyzed by Tolman et al.²³ based on the measurement of several dipolar couplings in one alignment medium. The residue specific internal GDO is defined as the ratio between the local and the overall alignment tensor (index o) (see eq 2 in ref 23):

$$\vartheta(\text{int}) = \sqrt{\frac{\sum_{ij} S_{ij}^2}{\sum_{ij} S_{ij,o}^2}} \quad (10)$$

where S_{ij} are the elements of the Saupe matrix. This leads to

$$\vartheta(\text{int}) = \frac{|\frac{1}{2}\sqrt{(4+3R^2)} \cdot S_{zz}|}{|\frac{1}{2}\sqrt{(4+3R_o^2)} \cdot S_{zz,o}|} \quad (11)$$

where R is the rhombicity ($R = (S_{xx} - S_{yy})/S_{zz}$), and S_{zz} is the axial component of the alignment tensor. If the rhombicity R is identical to R_o , the GDO is reduced to $S_{zz}/S_{zz,o}$.

In contrast to our S_{axial} , the GDO is sensitive to all motions affecting the amino acid residue, while a rotation of the amino acids around the average orientation of the NH vector is invisible in our analysis. However, anisotropy of motion only marginally affects the GDO. Even if the rhombicity is different for the overall and the fragment specific Saupe matrixes, the influence of the rhombicity is minor. The maximum change from $R = 2/3$ to $R = 0$ for the individual fragment or the reverse would change the GDO by 15%, while a change of R by 0.1 invariably leads to a change of the GDO by less than 1%. Thus, the GDO is quite insensitive to the motional anisotropy. This is in contrast from our approach as elaborated in the previous paragraph.

Experimental Section

¹⁵N and ¹⁵N,¹³C-labeled ubiquitin was purchased from VLI Research, Inc. (Malvern, PA) and used without further purification. All samples of ubiquitin between 1.5 and 3 mg were dissolved in 10 mM phosphate-

buffer pH 6.5 (H₂O/D₂O 90/10) in a 300 μ L Shigemi microcell tube. All experiments were recorded on either Bruker-DRX-600 MHz or Bruker-DRX-800 MHz spectrometers (Bruker AG, Rheinstetten, Germany) equipped with TXI HCN z -grad probes (measurement temperature was set to 303 K for all experiments). All spectra were processed using XWINNMR 2.6 (Bruker AG, Karlsruhe, Germany) and FELIX 98.0 or FELIX 2000 (MSI, San Diego, USA).

Liquid Crystal Media. Alignment of the protein was achieved using the following bicelles:^{41,42} CHAPSO/DLPC (1:5; 5%), CHAPSO/DLPC/CTAB (10:50:1; 5%), CHAPSO/DLPC/CTAB (10:50:1; 4%), CHAPSO/DLPC/SDS (10:50:1; 5%).^{43–45} CHAPSO/DLPC was purchased from Sigma (St. Louis, MO), SDS was purchased from Merck (Darmstadt, Germany), and CTAB was purchased from ACROS (New Jersey, USA) and used without further purification. Dipolar couplings of ubiquitin in DHPC/DMPC and DHPC/DMPC/SDS were taken from the literature.³⁹

In addition to bicelle media, other liquid crystalline media were used to obtain NH dipolar couplings in ubiquitin. For the measurement using purple membrane fragments (bacteriorhodopsin)^{46,47} (2 mg/mL), the salt concentration was increased up to 100 mM NaCl to decrease the electrostatic interaction between the highly charged bacteriorhodopsin and ubiquitin. For the same reason, 50 mM NaCl was used with Pf-1 phages (5 mg/mL, 50 mM NaCl, ASLA Ltd., Riga, Latvia).^{48,49} Alignment was additionally achieved using surfactant lipids ((cetylpyridiniumbromide/hexanol = 1:1.33), 25 mM NaBr, 5%) commonly named Helfrich phases.^{50,51} NH dipolar couplings in polyacrylamide gels (7% paa) were taken from the literature.^{52,53}

Using the nonionic liquid crystal medium composed of *n*-dodecyl-penta(ethylene glycol) and *n*-hexanol,⁵⁴ dipolar couplings could additionally be obtained. The very small line widths comparable to those of the proton resonances in isotropic solution render this medium ideal for measuring other heteronuclear backbone dipolar couplings in proteins.

The determination of the alignment tensor and all other calculations were performed using the home written software DipoCoup¹³ and Mathematica 4.0 (Wolfram Res., Inc., Oxfordshire, U.K.) on PC or SGI computer systems.

All NH dipolar couplings were measured using the S³E-¹H,¹⁵N HSQC⁵⁵ pulse sequence. In addition, a ¹H,¹⁵N HSQC spectrum without decoupling during t_1 was recorded. $t_{1\max}$ was set to the average ¹⁵N T_2 relaxation time of 160 ms that was estimated by constant time ¹H,¹⁵N HSQC experiments and T_2 time measurements to achieve the best possible resolution.

MD Simulation. A MD simulation of native ubiquitin was carried out under periodic boundary conditions using the program CHARMM 24.⁵⁶ An energy-minimized all-atom representation of the X-ray structure of ubiquitin⁵⁷ was embedded in a cubic box with a side length

of 46.65 Å containing a total of 2909 explicit water molecules. The simulation was performed at a temperature of 300 K with an integration time step of 1 fs. Details of this simulation have been reported elsewhere.^{24,32}

The experimental dipolar couplings were used to test the MD run. Comparison of the experimental results with the MD trajectory was performed by using the 11 different alignment tensors for calculating theoretical dipolar couplings from the MD trajectory and comparing them with the experimental dipolar couplings. The RMSD values between the experimental and the theoretical dipolar couplings show that large differences occur in the less structured regions such as the β -turn (Leu8-Lys11) and around the prolines (Pro19, Pro37, Pro38). The dynamical features of the very flexible C-terminal part have a rather poor description in the calculated trajectory. However, the agreement between trajectory and experiment is rather good for the secondary structure elements. Visualization of the differences between the experiment and the trajectory can also be derived from the comparison of the experimental $\theta_{\text{eff}}, \phi_{\text{eff}}$ values and the trajectory-derived $\theta_{\text{av}}, \phi_{\text{av}}$ values (Supporting Information, Figure S1a,b). In the highly dynamic loop regions the average angle values derived from the trajectory do not agree with the experimental values. These differences are much larger than those using the NMR or the X-ray structure to calculate the $\theta_{\text{av}}, \phi_{\text{av}}$ values. Interestingly, the trajectory describes the N-terminal part of ubiquitin much better than the C-terminal part. In fact, the N-terminal secondary structural elements are notably stable and even retained in media that normally completely unfold proteins.⁵⁸

Error Analysis. In the following we investigate the errors of our analysis. Because of the inversion of the \hat{F} matrix in eq 3, the errors on the dipolar couplings were translated into errors on the average spherical harmonics from which all further results were derived. The error propagation critically depends on the sampling of the five dimensional vector space spanned by the \hat{F}_i vectors. In an optimal situation, five alignment media would provide five orthogonal vectors. However, as will be found, this ideal situation cannot readily be realized experimentally. We measured the degree of nonsingularity of the \hat{F} matrix by calculating its singular values and the ratio between the largest and the smallest singular value (condition number). Ideally, the condition number is close to 1; in reality, however, the condition number is significantly larger than 1.

The error on the experimental dipolar couplings is ± 0.5 Hz (the errors in different media slightly depend on the signal-to-noise ratio). The isotropic couplings are measured using the HSQC- J technique that allows the measuring of the couplings with higher accuracy. Using all 11 experimental dipolar couplings, an average statistical error of 2.2% on the spherical harmonics ($\bar{Y}_{2M}(\theta, \phi)$) is found, with the largest error being 3.7% on one of the spherical harmonics. This yields a statistical error of the dipolar order parameter \bar{S}_{rdc} that is smaller than 2%, the largest statistical error being 3.2% on a single spherical harmonic. It should be noted that this analysis explicitly addresses only the statistical errors, while potential systematic errors are ignored.

Similar errors are obtained if only five or six alignment media are included. The optimal combination of six or five alignment media (Table 1) yields an average statistical error on the dipolar order parameter of 2.2% and 3.1%, with the largest error on the spherical harmonics being 4.2% and 6%, respectively. The largest possible error on the dipolar order parameter is 3.5% and 4.4%. Thus, the optimal

- (41) Sanders, C. R.; Schwonek, J. P. *Biochemistry* **1992**, *31*, 8898–8905.
 (42) Sanders, C. R., II; Hare, B. J.; Howard, K. P.; Prestegard, J. H. *Prog. Nucl. Magn. Reson. Spectrosc.* **1994**, *26*, 421–444.
 (43) Wang, H.; Eberstadt, M.; Olejniczak, T.; Meadows, R. P.; Fesik, S. W. *J. Biomol. NMR* **1998**, *12*, 443–446.
 (44) Losonczi, J. A.; Prestegard, J. H. *J. Biomol. NMR* **1998**, *12*, 447–451.
 (45) Ottinger, M.; Bax, A. *J. Biomol. NMR* **1998**, *12*, 361–372.
 (46) Sass, J.; Cordier, F.; Hoffmann, A.; Rogowski, M.; Cousin, A.; Omichinski, J. G.; Lowen, H.; Grzesiek, S. *J. Am. Chem. Soc.* **1999**, *121*, 2047–2055.
 (47) Koenig, B. W.; Hu, J.-S.; Ottinger, M.; Bose, S.; Hendler, R. W.; Bax, A. *J. Am. Chem. Soc.* **1999**, *121*, 1385–1386.
 (48) Hansen, M. R.; Mueller, L.; Pardi, A. *Nat. Struct. Biol.* **1998**, *5*, 1065–1074.
 (49) Clore, G. M.; Starich, M. R.; Gronenborn, A. M. *J. Am. Chem. Soc.* **1998**, *120*, 10571–10572.
 (50) Prosser, S. R.; Losonczi, J. A.; Shiyonovskaya, I. V. *J. Am. Chem. Soc.* **1998**, *120*, 11010–11011.
 (51) Barrientos, L. G.; Dolan, C.; Gronenborn, A. M. *J. Biomol. NMR* **2000**, *16*, 329–337.
 (52) Sass, J.; Musco, G.; Stahl, S. J.; Wingfield, P. T.; Grzesiek, S. *J. Biomol. NMR* **2000**, *18*, 303–309.
 (53) Tycko, R.; Blanco, F. J.; Ishii, Y. *J. Am. Chem. Soc.* **2000**, *122*, 9340–9341.
 (54) Rückert, M.; Otting, G. *J. Am. Chem. Soc.* **2000**, *122*, 7793–7797.
 (55) Meissner, A.; Duus, J. O.; O. W., S. *J. Biomol. NMR* **1997**, *10*, 89–94.

- (56) MacKerell, A. D. J.; Bashford, D.; Bellott, M.; Dunbrack, R. L. J.; Evanseck, J. D.; Field, M. J.; Fischer, S.; Gao, J.; Guo, H.; Ha, S.; Joseph-McCarthy, D.; Kuchnir, L.; Kuczera, K.; Lau, F. T. K.; Mattos, C.; Michnick, S.; Ngo, T.; Nguyen, D. T.; Prodhom, B.; Reiher, W. E. I.; Roux, B.; Schlenkerich, M.; Smith, J. C.; Stote, R.; Straub, J.; Watanabe, M.; Wiórkiewicz-Kuczera, J.; Yin, D.; Karplus, M. *J. Phys. Chem. B* **1998**, *102*, 3586–3616.
 (57) Vijay-Kumar, S.; Bugg, C. E.; Cook, W. J. *J. Mol. Biol.* **1987**, *194*, 531–544.
 (58) Brutscher, B.; Brüschweiler, R.; Ernst, R. R. *Biochemistry* **1997**, *36*, 13043–13053.

selection of six alignment media leads to similar results as the combination of all 11 alignment media.

Using the information provided exclusively by the bicelle media, the error propagation is less favorable. The largest error on the spherical harmonics is 56.6% (average statistical error 26.7%), and the statistical average error of the dipolar order parameter is 22.7%. Thus, with the six optimal or 11 used alignment media, the errors are low enough to obtain statistically significant conclusions.

Results

Measurement of Different Alignment Tensors. As mentioned in the Introduction, the alignment tensors must be sufficiently different so that the error propagation of the experimental dipolar couplings does not transform into an exceedingly large error on the averaged spherical harmonics $\langle Y_{2M}(\theta, \varphi) \rangle$, and so that the derivation of the θ_{eff} and ϕ_{eff} angles is faithful. Therefore, a major objective of the experimental work was to find alignment media that yield a sufficiently small condition number. The main axes of the alignment tensor with respect to the molecular frame were experimentally determined for nearly all alignment media used in this paper. Although the optimal media found for ubiquitin may not be optimal for other proteins, similarities of alignment tensors from different alignment media will most probably be independent of the protein. This was already seen for other proteins that are currently studied in our laboratory. For 11 alignment media, the alignment tensors in the molecule fixed coordinate system (Supporting Information, Figure S2) were determined. First, dilute liquid crystal media made from phosphocholines commonly referred to as bicelles^{2,41,42,59} were used. The bicelles can be charged by additives that introduce electrostatic interactions between the biomacromolecule and the bicelles and thus rotate the orientation of the tensor. Using CTAB (cetyltrimethylammoniumbromide) the bicelles are positively charged, while SDS (sodium dodecyl sulfonate) introduces a negative charge. Unfortunately, the tensor did not change considerably. As expected, there is also no difference when changing the mixture of the bicelles from CHAPSO/DLPC to DHPC/DMPC. This supports the notion that the shape rather than the charge distribution of the protein determines the alignment. This can also be derived from the small effect induced by the charged bicelles. Therefore, it was more important to find other experimental approaches to obtain sufficiently different orientations of the alignments. This was achieved using Pf-1 phage,⁴⁸ purple membrane (bacteriorhodopsin),^{46,47} Helfrich phase surfactant lipids,^{50,51} uncharged, nonionic *n*-dodecyl-penta(ethylene glycol)/*n*-hexanol phase,⁵⁴ and polyacrylamide gel^{52,53} for alignment. Some of these methods introduce much more charge onto the liquid crystals and therefore lead to bigger changes of the alignment tensors. By comparing the different phases, interesting equivalences of media for ubiquitin alignment were found. For example, the uncharged CHAPSO/DLPC bicelles and the nonionic *n*-dodecyl-penta(ethylene glycol)/*n*-hexanol phase yielded almost the same orientation of the alignment tensor in the molecular frame. Thus, for these two alignment media, the mechanism of alignment appears to be based on shape and not on the charge of the protein. This observation is also supported by the sharp lines of the spectra in these liquid crystal media and is additionally confirmed by unchanged transverse relaxation times (T_2) as compared to those in isotropic aqueous solution.

(59) Bax, A.; Tjandra, N. *J. Biomol. NMR* **1997**, *10*, 289–292.

In all charged liquid crystal media, the line widths are broader due to decreasing T_2 times and larger interaction with the orienting media. Both positive and negative charge on the alignment media induce a T_2 effect. For ubiquitin, a larger variation of the orientation of the alignment tensor was found when we measured in completely different alignment media rather than modifying one alignment method, for example, by addition of charges (CTAB or SDS in bicelle media). For example, using bicelle media alone provided the following scaled singular values: 3.889, 1.248, 0.479, 0.103, and 0.026 yielding a condition number of 152.1. All 11 alignment media, however, yielded the scaled singular values: 4.909, 2.260, 0.844, 0.675, and 0.594 and a condition number of 8.2. Table 1 contains the set of media with the smallest fifth singular value and the largest condition number for 5–11 alignment media used. It is interesting to note that the condition number for the optimal set of six alignment media is the smallest condition number, which is also smaller than that found for 11 alignment media. Because the absolute values of the singular values are responsible for the error propagation, the 11 media are still better than the six. For ubiquitin, DMPC/DHPC, CHAPSO/DLPC/SDS, bacteriorhodopsin, Pf-1 phages, the *n*-dodecyl-penta(ethylene glycol)/*n*-hexanol phase, and the Helfrich phases yielded the optimum information. Whether these alignment media will prove equally useful for other proteins remains to be seen. It should be noted, however, that although ubiquitin is quite stable and therefore compatible with many alignment media, it also has major drawbacks for alignment since it has an almost spherical shape and little charge due to its pI of 7.6.

In the following analysis we used only those residues for which dipolar couplings could be obtained in enough different media that the condition number was smaller than 10 to obtain statistically relevant data. To decrease the condition number even further, more alignment media would need to be measured. New media are found on a regular basis,⁶⁰ and therefore it is not unlikely that five or more alignment media can be found also for other biomolecules.

An alternative would be the measurement of several dipolar couplings in the peptide plane.⁶¹ However, there are drawbacks to this method as well. Other dipolar couplings beside the NH dipolar couplings are often less accurately measured due to smaller gyromagnetic ratios and longer distances, and, therefore, smaller dipolar coupling constants and their associated internuclear distances need to be accurately calibrated to exclude overestimation of motional anisotropies. N–H internuclear distances are well calibrated and understood.³⁹ The estimation of internuclear distances is critical. This was found when using chemical shielding anisotropies and dipolar couplings for structure calculation.⁶²

Extraction of θ_{eff} and ϕ_{eff} and Comparison with Different Structures of Ubiquitin and the MD Trajectory. As described in the Introduction, $\theta_{\text{eff}}, \phi_{\text{eff}}$ can be calculated by using eqs 4, 8, and 9. The best agreement is seen between the effective orientations ($\theta_{\text{eff}}, \phi_{\text{eff}}$) and the average vector orientation ($\theta_{\text{av}}, \phi_{\text{av}}$) using the NMR structure that was already refined against two

(60) Desvaux, H.; Gabriel, J.-C. P.; Berthault, P.; Camerel, F. *Angew. Chem.* **2001**, *113*, 387–389.

(61) Fushman, D.; Ghose, R.; Cowburn, D. *J. Am. Chem. Soc.* **2000**, *122*, 10640–10649; Cornilescu, G.; Bax, A. *J. Am. Chem. Soc.* **2000**, *122*, 10143–10154.

(62) Cornilescu, G.; Bax, A. *J. Am. Chem. Soc.* **2000**, *122*, 10143–10154.

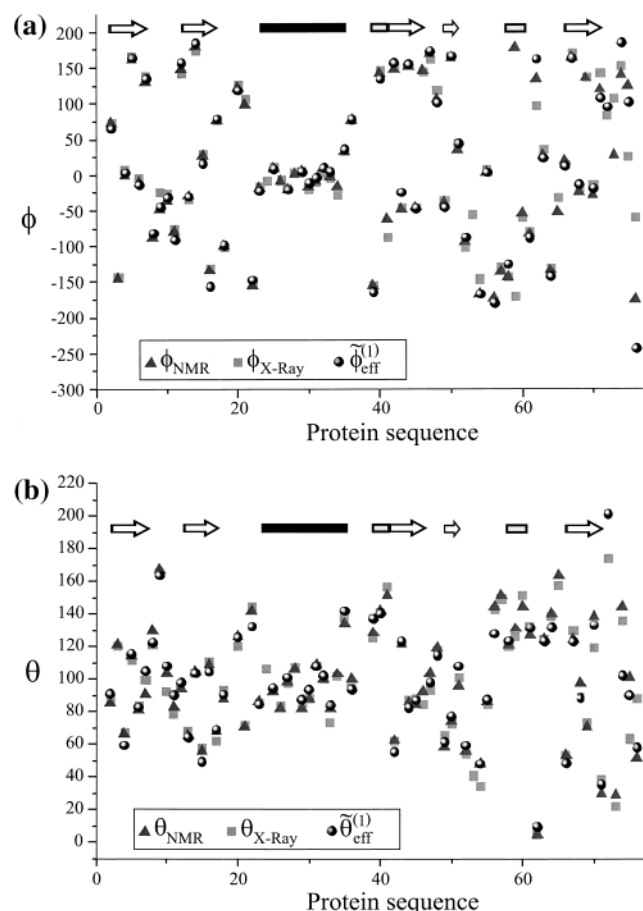


Figure 2. Comparison of the effective orientations of the NH vectors ϕ (a) and θ (b). The black spheres show the experimental model-free derived orientations calculated using eq 4. The triangles show the orientation of the NH vectors in the NMR structure, and the squares show the orientations in the X-ray structure.

sets of dipolar couplings.^{38,40} The NMR structure was also used for the back calculation of the alignment tensors. The orientations of the NH vectors derived using eq 4 differ slightly from those obtained in the three structures (trajectory, X-ray,⁵⁷ and NMR⁴⁰), especially in the very mobile regions: the C-terminal part, the first loop (Leu8–Lys11) between the two β -strands, around glycine 47 and glycine 53 (Figure 2a,b and Supporting Information). These are also the residues with the lowest GDO in the analysis of Tolman et al.²³

Absolute Overall Scaling. For all residues for which a sufficient number of dipolar couplings were available, and thus the condition number was smaller than 10, we were able to calculate the averaged spherical harmonics from eq 3. The order parameter derived from the $\langle \tilde{Y}_{2M}(\theta, \phi) \rangle$ values according to eq 7 can produce \tilde{S}_{rdc}^2 that can be larger than 1 for residues which are less mobile than the average residues. This unusual behavior of the order parameter \tilde{S}_{rdc}^2 is due to the principal component of the alignment tensors \tilde{D}_{izz} absorbing the average motion of all NH vectors in the protein. However, the order parameter S_{rdc}^2 that includes this average motion will be limited to a maximum of 1. Thus, we obtain S_{rdc}^2 by the scaling of \tilde{S}_{rdc}^2 with a constant factor whose derivation is described below. For 43 out of 76 residues, the condition number is below 10, and the order parameters \tilde{S}_{rdc}^2 range between 0.108 (Gly 76) and 1.62 (Glu 18) using the magnitude of the alignment tensors as obtained

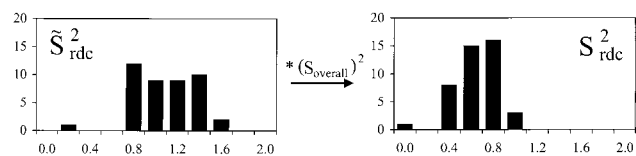


Figure 3. Histogram of the distribution of the order parameter \tilde{S}_{rdc}^2 (left). The distribution varies between 0.18 and 1.62. Scaling of the distribution by division by $S_{\text{overall}} = 0.78$ such that the maximal S_{rdc}^2 is 1 leads to the distribution of S_{rdc}^2 (right).

by direct fitting of the experimental dipolar couplings to the static NMR structure (Figure 3).

To obtain the nonscaled dipolar order parameters S_{rdc}^2 from \tilde{S}_{rdc}^2 , the value of S_{overall} that reflects the overall dynamics absorbed by the alignment tensors needs to be known. The sequence averaged $\sqrt{\langle S_{\text{rdc}}^2 \rangle}$ order parameter is the S_{overall} scaling parameter. This overall scaling S_{overall} cannot be derived from the experimental dipolar couplings in a unique way. Because dipolar couplings display motions over a very large time range, the expected value is unclear. We present three approaches to derive S_{overall} values for ubiquitin.

The distribution of the nonscaled dipolar order parameters \tilde{S}_{rdc}^2 yields an average of 1 and a maximum of 1.62 corresponding to the largest dipolar order parameter extracted. By scaling the largest experimental order parameter to 1, the average of the dipolar order parameter is $S_{\text{overall}} = 0.78$.

The second approach relies on the assumption that S_{rdc}^2 is smaller than the relaxation-derived Lipari–Szabo order parameter S_{LS}^2 , since S_{rdc}^2 is also sensitive to motions slower than the overall tumbling correlation time. The largest experimental \tilde{S}_{rdc}^2 values are found for the helix indicating that this is the most rigid secondary structural element in ubiquitin. Because residues 23 and 25 show conformational exchange,³⁵ only residues 24, 26, 28, 29, and 32 were used for the following analysis. The average S_{LS}^2 value was found to be 0.89 ± 0.02 for the helix residues from relaxation measurements.^{30–32} A fixed τ_c value of 4.05 ns, a ^{15}N CSA of -160 ppm, and a r^{NH} distance of 1.02 Å were used. Because the largest \tilde{S}_{rdc}^2 is found for the NH vectors of the helix and $S_{\text{rdc}}^2 \leq S_{\text{LS}}^2$ should be fulfilled, the most conservative assumption corresponds to the limiting case of $S_{\text{rdc}}^2 = S_{\text{LS}}^2$, where S_{overall} is set such that $\tilde{S}_{\text{rdc}}^2 S_{\text{overall}} = S_{\text{rdc}}^2 = S_{\text{LS}}^2$ for the NH vector with the largest $\tilde{S}_{\text{rdc}}^2/S_{\text{LS}}^2$ ratio (Ile 30). Fulfilling the equation for the residue with the largest ratio in the helix yields an overall scaling factor of $S_{\text{overall}} = 0.78$, which reproduces the value from the first approach.

The third approach relies on the calculation of alignment tensors based on dipolar couplings that are less sensitive to dynamics. H,H couplings that depend on larger distances are less scaled by motion than are NH dipolar couplings. This was also shown by analyzing the MD trajectory where $S_{\text{LSNH}} = 0.9$, $\tilde{S}_{\text{LSNH}\beta} = 0.93$, and $\tilde{S}_{\text{LSNH}\alpha} = 0.95$ were found. H,H dipolar couplings can be measured by the J_{HH} -NOESY method.⁶³ Although we showed that the measurement of the H,H dipolar couplings is highly accurate, the difference between the experimental dipolar couplings $D_{\text{HH}}^{\text{exp}}$ and the dipolar couplings calculated from the ubiquitin structure $D_{\text{HH}}^{\text{theo}}$ using the D_{NH} derived alignment tensor was quite large. This was also found

(63) Peti, W.; Griesinger, C. *J. Am. Chem. Soc.* **2000**, *122*, 3975–3976.

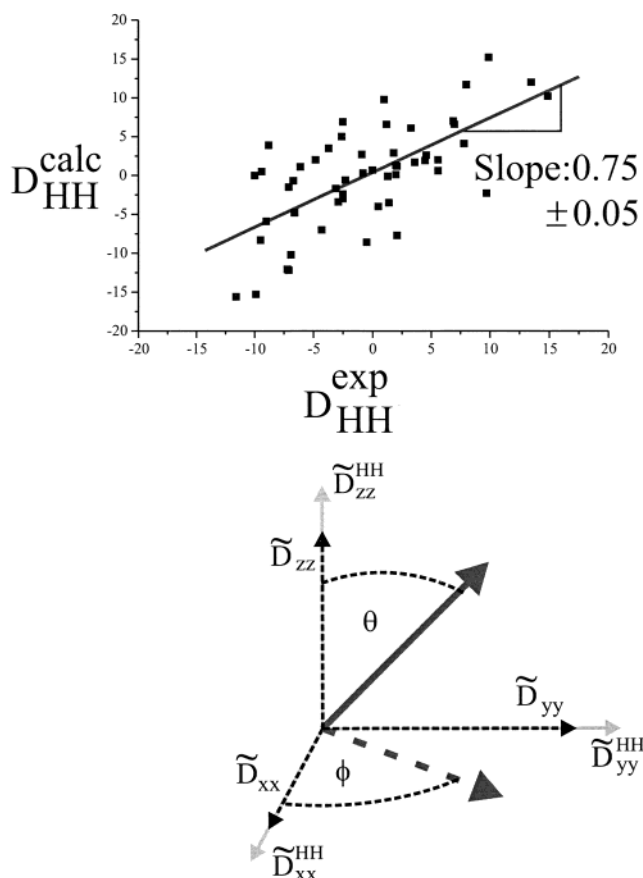


Figure 4. Linear regression of experimental $D_{\text{HH}}^{\text{exp}}$ and calculated $D_{\text{HH}}^{\text{calc}}$ proton-proton dipolar couplings. The experimental couplings were measured using the J_{HH} -NOESY experiment. The calculated couplings were derived from the ensemble of NMR structures using an alignment tensor (\tilde{D}_{zz} , \tilde{D}_{yy} , \tilde{D}_{xx}) back-calculated from the same structure and the NH dipolar couplings. The slope of the correlation is 0.75 ± 0.05 indicating that the NH dipolar coupling derived alignment tensor is smaller by this factor than the effective alignment tensor for the HH dipolar couplings (D_{zz}^{HH} , D_{yy}^{HH} , D_{xx}^{HH}).

when using the ensemble of NMR-derived structures of ubiquitin.^{38,40} However, the $D_{\text{HH}}^{\text{exp}}$ and $D_{\text{HH}}^{\text{theo}}$ could be correlated. The slope of the correlation was 0.75 indicating that the NH-derived alignment tensor used for the prediction of the H,H dipolar couplings was too small and that the H,H vectors experience a larger alignment tensor (Figure 4). This result depends on the selection of the dipolar couplings. This factor is 0.6 taking only $\text{H}^{\text{N}}\text{H}^{\beta}$ couplings into account, and 0.78 when only $\text{H}^{\text{N}}\text{H}^{\alpha}$ dipolar couplings are used. The $\text{H}^{\text{N}}\text{H}^{\alpha}$ dipolar couplings are expected to be the most reliable couplings since their distance variation only depends on the backbone φ torsion angle fluctuations. Additionally, the $\text{H}^{\text{N}}\text{H}^{\beta}$ dipolar couplings depend on the side chain χ_1 torsion angle.

There is further evidence that the alignment tensor derived from NH dipolar couplings experiences motion-induced scaling beyond what is expected from S_{LS} values. Tolman et al. compared the alignment tensor derived from RDCs with the one derived from pseudocontact shifts and found that they differ by about 20% in cyanometmyoglobin.¹⁶

A different explanation⁶³ was checked by a second, more detailed analysis with the same results.¹⁷ The scaling factor of 0.8 is similar to the scaling factor found in our analysis ($S_{\text{overall}} = 0.78$).

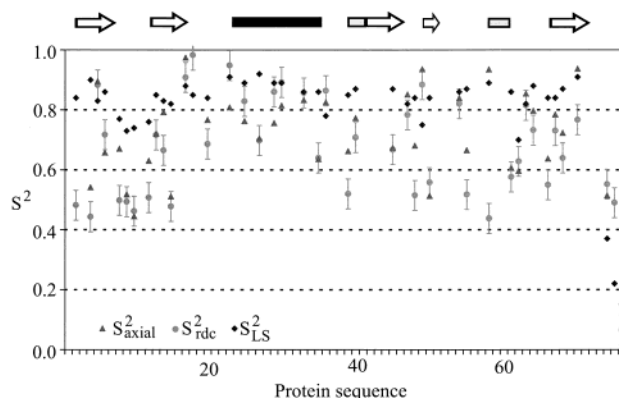


Figure 5. Comparison of the three order parameters discussed in the text. S_{rdc}^2 and S_{axial}^2 are order parameters derived from the dipolar couplings. They reflect structural variation up to the milliseconds range. S_{LS}^2 is the relaxation derived order parameter that describes motions faster than the reciprocal correlation time (4 ns for ubiquitin at 30 °C).

Comparable results as the ones reported by Prestegard et al. were obtained on the protein calbindin $\text{D}_{9\text{k}}$ ^{64–66} complexed with different paramagnetic lanthanides including Ce(III), Yb(III), and Dy(III). The overall scaling of the RDC-derived alignment tensor was found to be between 5% and 50%⁶⁷ as compared to the pseudocontact derived alignment tensor. Simple analytical models indicate a distance-dependent increase of the pseudocontact shift-derived alignment tensor. Thus, if short-range H^{N} protons are also included, the pseudocontact shift-derived alignment tensor is systematically reduced. The overall scaling factor of 0.78 found in the present study fits well with these findings.

As a consequence of these facts, a substantial part of motion of ubiquitin occurs on time scales slower than the overall tumbling correlation time τ_c .

As displayed in Figure 5, the dipolar order parameter S_{rdc} is smaller than the axial dipolar order parameter S_{axial} ; however, both are smaller than the order parameters from relaxation studies S_{LS} (sequence average: $\langle S_{\text{LS}} \rangle = 0.89$; $\langle S_{\text{axial}} \rangle = 0.85$; $\langle S_{\text{rdc}} \rangle = 0.78$). In Figure 6, the order parameters are displayed, using different colors, on the structure of ubiquitin. There are also a few residues that have larger S_{rdc}^2 than S_{LS}^2 values. Val 5, Val 17, and Ile 23 have S_{rdc}^2 values that are larger than their S_{LS}^2 values but are still in the error range of the S_{rdc}^2 values. Nevertheless, Glu 18, Ile 36, and Gln 49 have S_{rdc}^2 values that are larger than the corresponding S_{LS}^2 values, including the error. Interestingly, both Glu 18 and Ile 36 precede a proline residue (Pro 19 and Pro 37). At present, there is no satisfactory explanation for this effect. It might be due to an even smaller S_{overall} . The axial order parameter S_{axial} was correlated with the internal GDO values calculated by J. R. Tolman.²³ On average, the GDOs and the S_{axial} order parameters have comparable values (Figure 7).

S_{axial} only reports on the axial part of the motion; thus, the inequality $S_{\text{axial}} \geq S_{\text{rdc}}$ should hold. Furthermore, for a rigid vector, $S_{\text{axial}} = S_{\text{rdc}} = 1$ (Appendix). Indeed, we find that S_{rdc} is smaller than S_{axial} ($S_{\text{axial}} \geq S_{\text{rdc}}$) (Figure 5). Therefore, it is not

(64) Bax, A.; Tjandra, N. *Nat. Struct. Biol.* **1997**, *4*, 254–256.

(65) Allegrozzi, M.; Bertini, I.; Janik, M. B. L.; Lee, Y. M.; Lin, G. H.; Luchinat, C. *J. Am. Chem. Soc.* **2000**, *122*, 4154–4161.

(66) Bertini, I.; Felli, I. C.; Luchinat, C. *J. Biomol. NMR* **2000**, *18*, 347–355.

(67) Bertini, I.; Janik, M. B. L.; Liu, G. H.; Luchinat, C.; Rosato, A. *J. Magn. Reson.* **2001**, *148*, 23–30.

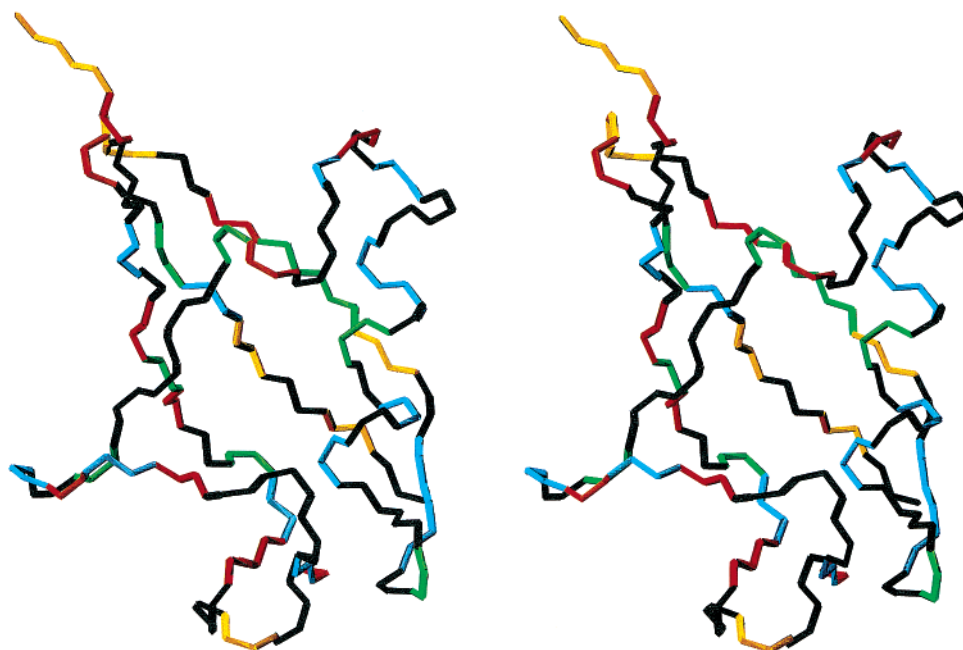


Figure 6. Stereo plot of ubiquitin where the different S_{rdc}^2 values are color coded onto the structure with gold $S_{\text{rdc}}^2 < 0.5$, dark orange $S_{\text{rdc}}^2 < 0.55$, orange red $S_{\text{rdc}}^2 < 0.65$, green $S_{\text{rdc}}^2 < 0.75$, and light blue $S_{\text{rdc}}^2 > 0.75$.

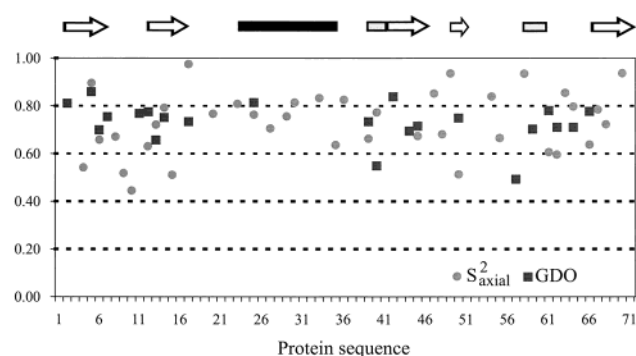


Figure 7. Plot of the GDO of Tolman et al. and the S_{axial}^2 parameters along the protein sequence. Both order parameters reflect axially symmetric motion.

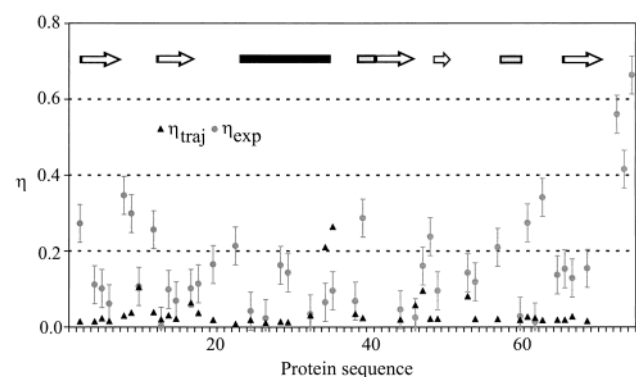


Figure 8. Representation of the parameter η along the ubiquitin sequence. The anisotropy of the orientational distribution derived from the experimental dipolar couplings and the trajectory is shown. The anisotropy found in the experiment is much larger than that found in the trajectory. This is especially true for the loops, bends, and β -sheet regions.

surprising that the anisotropy of the motion is quite large in some regions of ubiquitin including the loops and especially in the very flexible C-terminus. On average, the η value is 0.16, where amino acids in the nonsecondary structure elements show

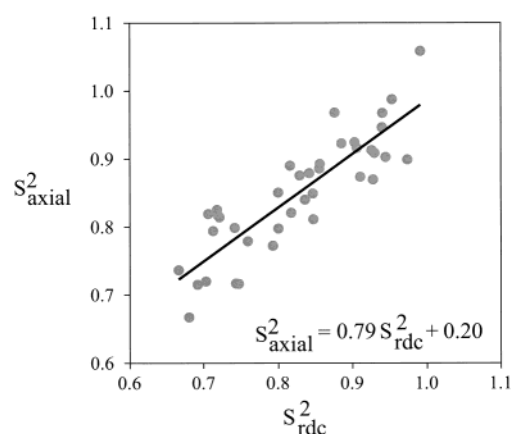


Figure 9. Correlation between S_{rdc}^2 and S_{axial}^2 . The slope is 0.79 indicating about 20% anisotropic motion in ubiquitin. This is in agreement with η displayed in Figure 8 averaged over the protein sequence.

quite large η values of up to 0.66 (Gly 76) (Figure 8). The average η value in the secondary structure elements is 0.12. This is in agreement with the finding that S_{axial}^2 is always larger than the S_{rdc}^2 values. If we correlate S_{axial}^2 and S_{rdc}^2 , an average slope of the linear regression of 0.8 is found which again indicates an average asymmetry of the motion of 20% ($S_{\text{axial}}^2 = 0.79 \cdot S_{\text{rdc}}^2 + 0.20$) (Figure 9). This contrasts greatly with the results from the 10 ns trajectory of ubiquitin where the asymmetry was on average 3.8%. However, this might be due to the different time ranges of motions that are sampled by the experimental data and the trajectory.

To obtain a more specific picture of the nature of the anisotropic motions, we performed the model-free analysis based on the $\langle \tilde{Y}_{2M}(\theta, \phi) \rangle$ values extracted from eq 3 where the average orientations $\theta_{\text{eff}}^{(1)}, \phi_{\text{eff}}^{(1)}$ and the amplitude of the axial motions $\langle \tilde{Y}_{20}(\theta', \phi') \rangle$ (Figure 10) are derived.

The information on the anisotropy of the motion is then reflected in the η and ϕ' values. ϕ' is the direction of the

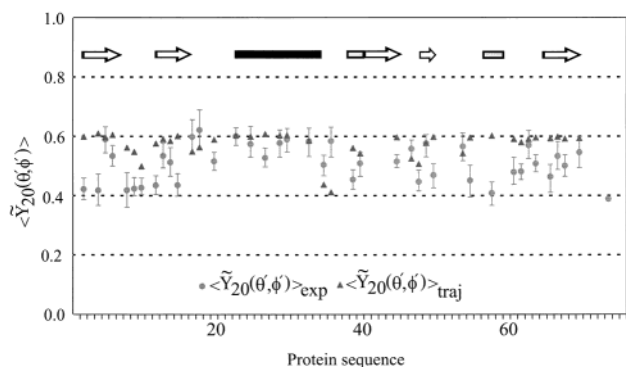


Figure 10. Experimental $\langle \tilde{Y}_{20}(\theta, \phi) \rangle$ values and the values derived from the trajectory along the ubiquitin sequence. The $\langle \tilde{Y}_{20}(\theta, \phi) \rangle$ values of the central helix in ubiquitin show the largest values. This is in accordance with the trajectory.

anisotropic motion in the x', y' plane for every residue. Figure 11a shows a $\bar{\phi}'$ plot for the experimental data and respective data derived from the trajectory. There is a good correlation of these values (Figure 11b) despite the considerable error on the experimental $\bar{\phi}'$ values.

The helix is quite immobile and has the highest experimental $\langle \tilde{Y}_{20}(\theta, \phi) \rangle$ values with small η values. This agrees well with the $\langle Y_{20}(\theta^{\text{traj}}, \phi^{\text{traj}}) \rangle$ extracted from the trajectory. Nevertheless, there is some detectable anisotropy of the motion. The average angle $\bar{\phi}'$ over the helix NH vectors is -20° with a distribution ranging from $+20^\circ$ to -55° . This indicates preferential mobility of all NH vectors in this direction. Whether these motions are correlated or uncorrelated cannot be derived from the dipolar couplings.

The β -sheets have considerably smaller $\langle \tilde{Y}_{20}(\theta, \phi) \rangle$ and S_{rdc} than S_{LS} values indicating large motions probably in the nanosecond to microsecond time scale because large $T_{1\rho}$ effects are absent in ubiquitin. The β -sheets exhibit a fair amount of anisotropic motion according to the η values. Similar to the helix, a clustering of the $\bar{\phi}'$ values around -130° in β -sheet 2 (residues 12–17) is found. This clustering of $\bar{\phi}'$ values can be found throughout the protein in other β -strands and also in loop regions. We are currently developing ways to translate these anisotropic parameters into motional models of secondary structure elements.

Interestingly, the experimentally derived $\bar{\phi}'$ values for the secondary structure elements and from the trajectory fit remarkably well with the exception of Ile 30, Thr 66, and His 68 (Figure 11b). These three residues are structurally particular. His 68 NH is involved in a weak hydrogen bridge across an antiparallel β -sheet; the NH of Thr 66 is not involved in an internal hydrogen bridge. The NH of Ile 30 is involved in a hydrogen bond, but this hydrogen bond is exposed to the water which could be the reason for the deviation between simulation and experimental finding. Thus, it appears that the direction of the anisotropic motion of NHs involved in internal hydrogen bridges is better represented by the molecular dynamics simulation than those of NHs that are not involved in internal hydrogen bridges. However, the amplitudes of the motions are too small in the molecular dynamics trajectory possibly due to the limited duration of the trajectory.

In the following we discuss some specific residues that are known for interesting dynamical features: The first loop

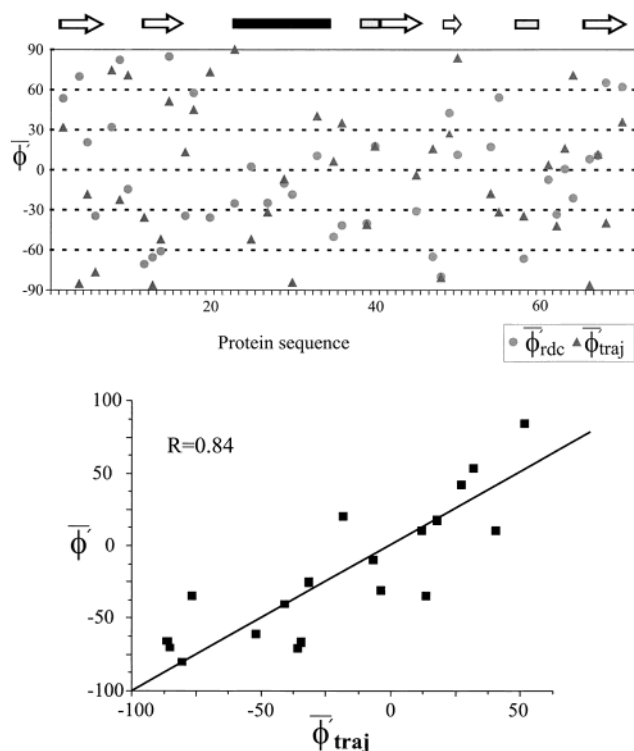


Figure 11. (a) Comparison of $\bar{\phi}'$ angles derived from the experimental dipolar couplings and from the trajectory. The values correlate quite well in the secondary structure elements except for the residues Ile 30, Thr 66, and His 68. The correlation plot shown in (b) has a correlation coefficient of $R = 0.84$ excluding the three outliers mentioned before.

consisting of the amino acid sequence Thr⁷-Gly⁸-Thr⁹-Gly¹⁰-Lys¹¹-Thr¹² connecting two β -strands of ubiquitin exhibits enhanced internal mobility as seen in all dynamical studies so far.^{30–32} The dipolar order parameters are also smaller for this loop (on average $S_{\text{rdc}} = 0.7$) than the average dipolar order parameter of 0.78 found in this analysis.

For those two residues that show slow conformational exchange based on relaxation experiments,³⁵ large dipolar order parameters were found. These are Ile 23 ($S_{\text{rdc}}^2 = 0.95$) and Asn 25 ($S_{\text{rdc}}^2 = 0.83$). Val 70 that also shows slow conformational exchange as observed in $T_{1\rho}$ measurements in supercooled water has no conspicuous RDC derived order parameter of $S_{\text{rdc}}^2 = 0.77$.⁶⁸

Possible Alternative Explanations. The amount of motion reflected in the dipolar order parameter is approximately twice that previously derived from relaxation measurements. These conclusions are based on several assumptions. Different conformations of the protein that are naturally present will induce varying alignment tensors. We assume in our analysis that averaging over these different alignment tensors leads to an overall alignment tensor that amounts to a uniform scaling for all alignment media. This cannot be proven with our measured data. However, whether the average structure of ubiquitin is changed in the different alignment media due to interactions with the alignment media can be checked. To check the integrity of the ubiquitin structure, we measured ¹⁵N- T_2 times and H,H-NOESY spectra of ubiquitin in a Helfrich phase, CHAPSO/

(68) Banci, L. *42nd ENC*; Orlando, FL, 2001.

(69) Skalicky, J. J.; Sukumaran, D. K.; Mills, J. L.; Szyperki, T. *J. Am. Chem. Soc.* **2000**, *122*, 3230–3231.

DLPC/CTAB 5% phase, and in isotropic solution. Helfrich phases were chosen because they induced the largest line broadening in the ubiquitin spectra. The CHAPSO/DLPC/CTAB 5% phase was chosen to represent the behavior of the bicelles as one of the most commonly used and most stable phosphocholine mixture. The NOESY spectra were recorded with mixing times that were adapted to the effective correlation time of ubiquitin in water and in the liquid crystal media. After the ^{15}N - T_2 time measurement, 2D NOESY spectra with ^{15}N - T_2 time adapted mixing times have been quantitatively analyzed. The NOESY mixing times were set according to $((\tau_{\text{m, isotropic}}/T_{2, \text{ isotropic}}) = (\tau_{\text{m, aligned}}/T_{2, \text{ aligned}}))$ since all rates relevant in the NOESY scale with the correlation time of the molecule, which in turn is proportional to the reciprocal ^{15}N - T_2 times. The fact that the NOEs recorded in the two phases differ at maximum by less than $\pm 6\%$ indicates that the structure of ubiquitin does not change upon binding in the liquid crystal medium (Helfrich phase $\pm 6\%$, CHAPSO/DLPC/CTAB phase $\pm 4.5\%$). The errors on the NOESY cross-peaks in the liquid crystal media are approximately 5%. The background noise is quite strong due to the liquid crystal media when compared with spectra recorded in isotropic solution. Thus, the NOESY cross-peak integrals between the aligned and the isotropic structure are not significant.

The ^{15}N - T_2 times are smaller in all regular secondary elements in the aligned phases. This indicates homogeneous interactions of the protein with the alignment media. For the Helfrich phase the ^{15}N - T_2 times of the C-terminal residues become larger than the isotropic values, which is presently not understood. It could indicate unfolding of the terminal β -sheet, which in turn could increase the time scale of mobility of the C-terminus. However, we do not see any indication of this from the NOEs in this region.

Another explanation that the alignment tensor is averaged due to the side-chain mobility of the protein can be excluded as this would affect all dipolar couplings in the same way. This is in disagreement with the proton–proton dipolar couplings.

We also assume that the dynamics of the protein do not change when we add it to the alignment phase. This was checked by measuring the ^{15}N - T_2 times which showed, at least for the secondary structure elements, similar scaling for all NHs involved in secondary structure elements.

To study the impact of the static reference structure on the results, the NH vector orientations $\theta_{\text{eff}}^{(1)}, \phi_{\text{eff}}^{(1)}$ were used in our analysis protocol. Although most of the changes in orientations were within a range of $\pm 10^\circ$, the back-calculated alignment tensors were less favorable for our analysis since the smallest singular value decreases by 20% which pushes the average condition number from 7.6 to 9.9. Nevertheless, the main conclusions hold for the changed alignment tensors: The \tilde{S}_{rdc}^2 values for the initial and the new tensors correlate very well ($R = 0.97$), meaning that the differences in motion for the different parts of the molecule are reproduced. However, the S_{overall} value derived from the new orientations would be smaller than 0.78, clearly indicating that this parameter requires support from other experimental input. It should also be noted that the new tensors exhibit a larger condition number, which increases the error of the analysis. Thus, a condition number of a maximum 10 is required to perform this part of the analysis.

Summary

We have shown that a model-free analysis of motion derived from NH dipolar couplings when measured in at least five or six media is possible (Table 1) due to the differences of the alignment processes. We have quantified the differences of the alignment tensors by the condition number and the singular values of the \hat{F} matrix. We have found that the average vector orientations derived from the measurement in the different alignment media deviate slightly from the previously known experimental and theoretical structures. In addition, we could derive average spherical harmonics for the NH vectors that describe the amplitude as well as the anisotropy of the motion. Using the spherical harmonics, we have derived a residual dipolar coupling order parameter that is found to deviate significantly from the relaxation derived Lipari–Szabo order parameter especially in the β -sheets and loops. This indicates that on the time scale slower than the tumbling correlation time, but faster than the detection limit of $T_{1\rho}$, considerable motion occurs. In accordance with this finding, the rather small sequence averaged $\langle S_{\text{rdc}} \rangle = S_{\text{overall}} = 0.78$ is smaller than the average Lipari–Szabo order parameter of $\langle S_{\text{LS}} \rangle = 0.9$. If we assume axial wobbling in a cone according to $(\frac{1}{2} \cos \alpha (1 + \cos \alpha) = S_{\text{axial}})$, the amplitude for the fast motion of $S_{\text{LS}} = 0.9$ would imply an opening half-angle of approximately 22° . The additional disorder $\langle S_{\text{rdc}} \rangle$ derived from the residual dipolar couplings calls for an additional wobbling in the cone-half-angle of about 24° .

From the analysis of the individual spherical harmonics, we observed a considerable amount of anisotropy in the motion. This effect is predominant in β -sheets and loops but less pronounced in helices. We have observed similarities of the directions of the anisotropic motions in secondary structure elements and agreement with the MD trajectory in this respect.

Acknowledgment. This work was supported by the DFG, MPG, and the Fonds der chemischen Industrie (to C.G.) and NSF Grant MCB-9904875 (to R.B.). All measurements were done at the Large Scale Facility for Biomolecular NMR at the University of Frankfurt, Germany. We would like to thank Hans-Jürgen Sass and Stephan Grzesiek (University of Basel, Switzerland) for the polyacrylamide gel dataset. We would also like to thank Prof. Dr. Dieter Oesterhelt (MPI for Biochemistry, Martinsried, Germany) for the bacteriorhodopsin samples. We also thank Dr. Tauseef R. Butt (VLI-Research) for sponsorship of ubiquitin samples.

Appendix

The transformation from eq 1 to eq 2 transforms the orientations in the individual alignment frames given by $\theta_i^{\text{at}}, \phi_i^{\text{at}}$ into orientations in the molecular frame given by $\theta^{\text{mol}}, \phi^{\text{mol}}$ by virtue of Wigner rotation matrices.

$$\frac{D_i^{\text{exp}}}{D_{i,zz}} = \sqrt{\frac{4\pi}{5}} \left(\langle Y_{20}(\theta_i^{\text{at}}, \phi_i^{\text{at}}) \rangle + \sqrt{\frac{3}{8}} R_i \left(\langle Y_{22}(\theta_i^{\text{at}}, \phi_i^{\text{at}}) \rangle + \langle Y_{2-2}(\theta_i^{\text{at}}, \phi_i^{\text{at}}) \rangle \right) \right) \quad (\text{A1})$$

$$\begin{aligned}
&= \sqrt{\frac{4\pi}{5}} \left(\sum_{M=-2}^2 e^{-iM\alpha^i} d_{M0}^2(\beta^i) \langle Y_{2,M}(\theta^{\text{mol}}, \phi^{\text{mol}}) \rangle \right) + \\
&\quad \sqrt{\frac{4\pi}{5}} \sqrt{\frac{3}{8}} R \left(\sum_{M=-2}^2 e^{-iM\alpha^i} d_{M2}^2(\beta^i) e^{-2i\gamma^i} \langle Y_{2,M}(\theta^{\text{mol}}, \phi^{\text{mol}}) \rangle + \right. \\
&\quad \left. e^{-iM\alpha^i} d_{M-2}^2(\beta^i) e^{2i\gamma^i} \langle Y_{2,M}(\theta^{\text{mol}}, \phi^{\text{mol}}) \rangle \right) \quad (\text{A2})
\end{aligned}$$

where $D_{i,zz}$ is the axial value of the dipolar couplings, R_i is the rhombicity of the alignment, and $\langle Y_{2M}(\theta, \phi) \rangle$ are the averaged spherical harmonics for a given NH vector:

$$Y_{20}(\theta, \phi) = \sqrt{\frac{5}{16\pi}} (3 \cos^2 \theta - 1);$$

$$Y_{2\pm 1}(\theta, \phi) = \pm \sqrt{\frac{15}{8\pi}} e^{\pm i\phi} \cos \theta \sin \theta;$$

$$Y_{2\pm 2}(\theta, \phi) = \sqrt{\frac{15}{32\pi}} e^{\pm 2i\phi} (\sin^2 \theta)$$

The superscript *at* describes the spherical harmonics in each of the alignment tensor frames. As mentioned in the text, the superscript *mol* describes the change of the coordinate system from the alignment tensor frame into the molecular frame brought about by the rotation about the three Euler angles α_i , β_i , and γ_i . This transformation defines the matrix $F_{i,M}$:

$$\begin{aligned}
F_{i,M} = &\sqrt{\frac{4\pi}{5}} \left(e^{-iM\alpha^i} d_{M0}^2(\beta^i) + \right. \\
&\left. \sqrt{\frac{3}{8}} R (e^{-iM\alpha^i} d_{M2}^2(\beta^i) e^{-2i\gamma^i} + e^{-iM\alpha^i} d_{M-2}^2(\beta^i) e^{2i\gamma^i}) \right) \quad (\text{3})
\end{aligned}$$

In the text θ and ϕ always refer to the reference frame of the molecule.

For the coordinate frame x', y', z' in which the $\langle \tilde{Y}_{20}(\theta', \phi') \rangle$ are maximized according to eq 4, the anisotropy of the motion is only reflected in the $\langle \tilde{Y}_{22}(\theta', \phi') \rangle$ and $\langle \tilde{Y}_{2-2}(\theta', \phi') \rangle$ averages. The averaged $\langle \tilde{Y}_{21}(\theta', \phi') \rangle$ and $\langle \tilde{Y}_{2-1}(\theta', \phi') \rangle$ values are zero, because for the maximum condition for $\langle \tilde{Y}_{20}(\theta', \phi') \rangle$ the derivatives with respect to any rotation about the primed axes $\partial \langle \tilde{Y}_{20}(\theta', \phi') \rangle / \partial \delta_{x', y', z'}$ must vanish. Because an infinitesimal rotation about the primed axes $(\delta_{x'}, \delta_{y'})$ is identical to the application of the angular momentum operators:

$$0 = \frac{\partial}{\partial \delta_{x'}} \langle \tilde{Y}_{20}(\theta', \phi') \rangle = \frac{L_x \langle \tilde{Y}_{20}(\theta', \phi') \rangle}{i\hbar} = \frac{\langle \tilde{Y}_{21}(\theta', \phi') \rangle + \langle \tilde{Y}_{2-1}(\theta', \phi') \rangle}{i\hbar} \quad (\text{A4})$$

$$0 = \frac{\partial}{\partial \delta_{y'}} \langle \tilde{Y}_{20}(\theta', \phi') \rangle = \frac{L_y \langle \tilde{Y}_{20}(\theta', \phi') \rangle}{i\hbar} = \frac{(\langle \tilde{Y}_{21}(\theta', \phi') \rangle - \langle \tilde{Y}_{2-1}(\theta', \phi') \rangle)}{\hbar} \quad (\text{A5})$$

we find that the $\langle \tilde{Y}_{21}(\theta', \phi') \rangle$ and $\langle \tilde{Y}_{2-1}(\theta', \phi') \rangle$ averages are zero.

There is no analytical expression for S_{axial} as a function of S_{rdc} and η . However, the empirical correlation $(\sqrt{4\pi/5} \langle Y_{20} \rangle) \cdot (S_{\text{axial}}) \approx S_{\text{rdc}}^2$ holds with a correlation coefficient of $R = 0.89$ for our experimental data.

Supporting Information Available: Graphical representation of the 11 alignment tensors, comparison of $(\theta_{\text{eff}}^{(1)}, \phi_{\text{eff}}^{(1)})$ with $(\theta_{\text{ave}}^{\text{traj}}, \phi_{\text{ave}}^{\text{traj}})$ (PDF). This material is available free of charge via the Internet at <http://pubs.acs.org>.

JA011883C